Computational Materials Science 170 (2019) 109151

Contents lists available at ScienceDirect

Computational Materials Science

journal homepage: www.elsevier.com/locate/commatsci

# Modeling of atomistic scale shear failure of Ag/MgO interface with misfit dislocation network

X.Q. Fu[a,d], L.H. Liang[b,*], Y.G. Wei[c,*]

[a] LNM, Institute of Mechanics, Chinese Academy of Sciences, Beijing 100190, China
[b] College of Mechanical and Electrical Engineering, Beijing University of Chemical Technology, Beijing 100029, China
[c] College of Engineering, Peking University, Beijing 100871, China
[d] School of Engineering Science, University of Chinese Academy of Sciences, Beijing 101408, China

ARTICLE INFO

*Keywords:*
Interface energy
Interface slip
Dislocation network
Atomistic simulation

ABSTRACT

Metal/ceramic interfaces have broad applications and misfit dislocation network (MDN) is a prominent feature of the equilibrium metal/ceramic interfaces. As one main failure mode, interface shear failure is strongly affected by the motion of MDN. In this work, we investigate the equilibrium interface structure and shear failure of Ag/MgO interface via atomistic simulation method. Periodically distributed in-plane strain field caused by MDN and severe strain concentration at dislocation node regions are found by strain analysis. During interface shearing, these dislocation nodes act as strong pinning points to the gliding motion of MDN, which leads to bending of dislocation lines. Besides, energy analysis shows the interface shear stress is largely dependent on the variation of misfit dislocation energy. To understand interface shear failure under more complex conditions, we study the effect of model thickness and shear direction further. Due to transformation of nodal structure, the shear strength of thick model eventually decreases by almost a quarter; shear failure along the direction of Burgers vector is found to be energetically favored, with the lowest interface shear strength. This work reveals the crucial role of MDN in interface shear process, and the theoretical understanding gives some hints to metal/ceramic interface design.

## 1. Introduction

Metal/ceramic interfaces have been the focus of research for more than five decades, due to their critical importance in many advanced engineering applications such as micro/nano-electronics, superconductors, protective coatings, etc. [1–6]. In general, the macro-mechanical characters of metal/ceramic composites are intimately linked with the interfacial properties at the atomic level. Due to lattice mismatch and orientation relationship between the two constituent materials, misfit dislocation network (MDN) is a prominent feature of many metal/ceramic interfaces [7,8]. As an inherent defect of the interface, MDN has significant influence on the interface microstructure, interface adhesion and interface failure mechanism.

The existence of misfit dislocations has been widely confirmed by experimental studies [3,9–11]. Early high-resolution transmission electron microscopy (HRTEM) researches showed the misfit dislocations at Ag/MgO interface formed a square network with orientations along ⟨1 1 0⟩ directions [9,10]. Owing to the limitation of measurement accuracy, experimental results were influenced by many factors such as temperature and metal layer thickness. Recently, with the development of spherical aberration (Cs)-correlated HRTEM, more precise microstructure information about the equilibrium metal/ceramic interfaces can be obtained [3,11]. Whereas, experimental researches mainly focus on the static characteristics such as interface structure, adhesive energy, and the distribution of interfacial stress/strain field. It is still challenging to investigate the atomic configuration of misfit dislocation network as well as its motion in interface dynamics.

Theoretical studies have been carried out almost exclusively by employing the continuum theory of dislocations, which cannot describe the structure of misfit dislocation core [12–15]. Besides, the theoretical solution will be more complicated if considering the interaction between misfit dislocations at the interface [14]. Computer simulation techniques such as molecular static/dynamics (MS/MD) simulations turn out to be good alternatives for studying interface misfit dislocations. Based on the second-nearest-neighbor modified embedded atom potential [16], the deformation mechanisms of several metal/nitride and metal/carbide nanolaminates were explored [17,18]. For the widely existing metal/oxide interfaces, a series of modified Rahman-

* Corresponding authors.
*E-mail addresses:* lianglh@lnm.imech.ac.cn (L.H. Liang), weiyg@pku.edu.cn (Y.G. Wei).

https://doi.org/10.1016/j.commatsci.2019.109151
Received 12 April 2019; Received in revised form 15 July 2019; Accepted 18 July 2019
Available online 22 July 2019
0927-0256/ 

Stillinger-Lemberg potentials (RSL2) has been successfully applied to study the structure of misfit dislocations at several metal/MgO and metal/$Al_2O_3$ interfaces [19,20]. However, researches on the motion of MDN at these metal/oxide interfaces are still scarce.

Both experimental and theoretical researches show that the effect of MDN on interface mechanical properties is manifold, such as strain hardening [17,18,21], pinning effect of the dislocation nodes [22,23], and local strain field caused by MDN [3,23]. The stress/strain concentration regions near the interface are "dangerous" regions, since stress-induced film cracking, buckling, or void nucleation typically occur there, which may lead to interface failure. Further, atomistic simulations reported thickness-dependent misfit dislocation energy and interface structure [24]. In-situ compression testing of CrN/Cu/Si(0 0 1) micro-pillars with 45° inclined interfaces also showed the average shear stress that initiated shear failure of the interfacial regions decreased with increasing metal interlayer thickness [23,25]. Then what is the shear failure mechanism of metal/ceramic interfaces containing MDN? Is the interfacial shear behavior affected by model thickness or shear direction?

In this work, we employ the atomistic simulation method to study the interface structure and shear mechanism of semi-coherent Ag/MgO interface with MDN. First, the interatomic potentials and interface model are introduced in Section 2. Second, the equilibrium interface structure is shown in Section 3. The residual strain field around the interface is analyzed in Section 3.1 and we calculate the interface energy and work of adhesion in Section 3.2. Third, results of interface shear are shown in Section 4. To be specific, interface traction-displacement relationship and relevant energy analysis are presented in Section 4.1 and Section 4.2; the effect of model thickness and shear direction are discussed in detail in Section 4.3 and Section 4.4. Finally, Section 5 gives a conclusion of this paper.

## 2. Interatomic potentials and interface model

### 2.1. Interatomic potentials

For Ag/MgO interface system, two kinds of interatomic potentials need to be given: interface potentials $\Phi_{Ag-Mg}$, $\Phi_{Ag-O}$, and bulk potentials $\Phi_{Ag-Ag}$, $\Phi_{Mg-Mg}$, $\Phi_{Mg-O}$, $\Phi_{O-O}$. In our simulations, interface potentials were fit into the modified Rahman-Stillinger-Lemberg (RSL2) form [27]:

$$\Phi r = D_0 e^{y\left(1-\frac{r}{R_0}\right)} + \frac{a_1}{1+e^{b_1(r-c_1)}} + \frac{a_2}{1+e^{b_2(r-c_2)}} + \frac{a_3}{1+e^{b_3(r-c_3)}} \quad (1)$$

For bulk potentials, $\Phi_{Ag-Ag}$ was also in RSL2 form [27]. MgO is an ionic crystal and each of its three pair potentials $\Phi_{Mg-Mg}$, $\Phi_{Mg-O}$ and $\Phi_{O-O}$ contains both short-range interaction part and long-range Coulomb interaction part $Q_{eff}^2/4\pi\varepsilon_0 r$. For Mg-Mg and O-O interaction, the short-range parts were taken as Morse form:

$$\Phi r = D_0\left(e^{-y\left(\frac{r}{R_0}-1\right)} - 2e^{-\frac{y}{2}\left(\frac{r}{R_0}-1\right)}\right) \quad (2)$$

For Mg-O interaction, the short-range part was taken as "Exp-Repulsive" form:

$$\Phi r = D_0 e^{y\left(1-\frac{r}{R_0}\right)} \quad (3)$$

It is not uncommon to utilize pair potentials to describe the atomic interactions across the interface [7,26]. In fact, these pair potentials, which were obtained from *ab initio* adhesive energies, had proven to be able to efficiently reproduce the basic elastic and energetic properties of bulk materials, as well as the adhesive energies of metal/ceramic interfaces [19,20,27]. The specific potential parameters can be referred to Ref. [28].

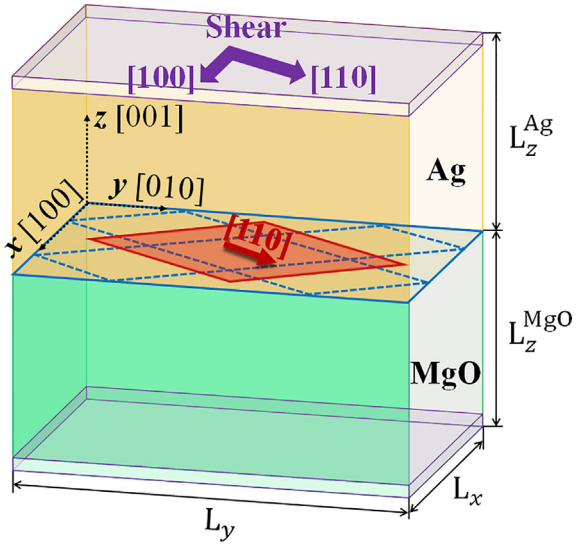


**Fig. 1.** Schematic of the Ag/MgO interface model with MDN (blue dashed lines). For interface shear along the [1 1 0] direction, the interface size is shown by the red area. For interface shear along the [1 0 0] direction, the interface size is shown by the blue frame. Last MLs of silver and magnesia (marked by the purple regions) are fixed boundary atoms.

### 2.2. Interface model

The schematic in Fig. 1 shows the computational model of semi-coherent Ag/MgO interface system. It has a cube-on-cube orientation relationship, which means that the cubic axis of the FCC Ag and rock-salt structure MgO are aligned, i.e., $[1\,0\,0]_{Ag}$ || $[1\,0\,0]_{MgO}$ (*x*-axis), $[0\,1\,0]_{Ag}$ || $[0\,1\,0]_{MgO}$ (*y*-axis), $[0\,0\,1]_{Ag}$ || $[0\,0\,1]_{MgO}$ (*z*-axis), and interface normal is parallel to the [0 0 1] crystal orientation. This orientation relationship is consistent with that experimentally observed on epitaxial Ag/MgO (0 0 1) interface [29]. Considering the lattice constant ratio between Ag and MgO ($a_{Ag}$ = 4.10 Å, $a_{MgO}$ = 4.32 Å), we constructed a (20 × 20):(19 × 19) interface model to obtain the misfit dislocation network.

In this work, interface shear along different directions were studied (Section 4.4) and for shearing along [1 1 0] and [1 0 0] directions, the interface sizes were taken as 11.6 nm × 11.6 nm and 16.4 nm × 16.4 nm respectively (shown by the red and blue areas in Fig. 1). This choice of dimension ensures the in-plane stresses caused by lattice mismatch in the Ag slab and MgO slab are the minimum. In order to investigate the effect of model thickness, we changed the thickness of Ag slab ($L_z^{Ag}$) and MgO slab ($L_z^{MgO}$) proportionally, and both $L_z^{Ag}$ and $L_z^{MgO}$ ranged from 10 unit lattices to 20 unit lattices. The interface model is periodic in *x*, *y* and *z* directions. To avoid spurious slab-slab interactions caused by periodic boundary condition, the Ag slab and MgO slab were separated by a vacuum region which was twice the thickness of the interface system.

### 2.3. Relaxation and deformation method

The MD simulations were performed using LAMMPS [30]. We visualized atomic structures and did strain analysis with OVITO [31]. The initial configuration was first relaxed via molecular static methods – the CG algorithm with a force convergence tolerance of $10^{-4}$ eVÅ$^{-1}$, followed by molecular dynamics relaxation through NPT ensemble at zero pressure and 1 K for 6 ps. After relaxation, the normal stresses $\sigma_{zz}$ in both Ag slab and MgO slab are zero, and the summation of the transverse stresses, $\sigma_{xx}$ and $\sigma_{yy}$, within the two crystals approaches zero (< 10 MPa).

Then the equilibrium interface structure was subjected to displacement controlled shear loading. The top Ag ML was moved

successively by a short distance (0.003 Å) along $x$ direction, and the energy of the mobile atoms was minimized after every loading step. During the interface shear process, the bottom boundary atoms were fixed and the top boundary atoms were allowed to move perpendicular to the interface. In this way, the boundary effect on dislocation motion is excluded.

In the present study Virial stress [32] was used for calculation of shear stress at the atomic level [33–35]. Note that the interface stress can be calculated by different methods, such as Virial stress, interface interaction force, and derivative of the total energy, which have been proven to be identical in our previous work [27]. Interface displacement $\delta_t$ was defined as the relative displacement between interfacial Ag ML and MgO ML along the shear direction. Shear loading will also induce small interface normal separation, thus $\delta_n$ as the normal displacement between interfacial Ag ML and MgO ML was calculated, too. Considering the Coulomb interactions, the potential cutoff was taken to be large (20 Å in this work) to comprise all electrostatic interactions for an atom, and Standard Ewald summation [36] was used to calculate long-range Coulomb interactions.

## 3. Equilibrium interface structure

### 3.1. Residual strain distribution around the interface

Due to the formation of misfit dislocations, non-uniform strains exist in both Ag and MgO near the interface. So we first analyzed the local strain field caused by MDN. Considering that atoms move mainly in the $x$-$y$ plane during the interface shear process, in-plane strain is discussed here. Taking the unrelaxed atomic structure as the reference configuration, the in-plane mean atomic strain is calculated as $\bar{\varepsilon} = 0.5\varepsilon_{ii}$, where $i = x, y$. Fig. 2(a) and (b) show the strain distribution in the vicinity of the interface from three-dimensional and two-dimensional perspectives, respectively.

From Fig. 2(a) one can see that Ag is compressed (negative strain) while MgO is stretched (positive strain) at node regions. In the region between nodes, Ag experiences tensile strain while MgO is subjected to compressive strain. Compared with metal, the strain in oxide is much smaller. Besides, the obvious in-plane tensile and compressive deformation is distributed in a small region near the interface – up to the fifth atomic layer. Experimental researches on the geometrical misfit dislocation of Cu/MgO interface have shown similar strain fields around the dislocation cores [3]. Beyond the range of five atomic layers, much smaller local strain is induced periodically in bulk Ag and MgO – mainly in the elastically softer Ag – by the interfacial MDN. In fact, this reflects the transformation of in-plane tensile zone and compressive zone.

For a more detailed observation of the strain distribution parallel to the interface, contour plot of $\bar{\varepsilon}$ in the first Ag ML adjacent to Ag/MgO interface is drawn in Fig. 2(b). It shows that the strain distributes periodically on the interface, depending on the location of dislocation network. Large compressive strain concentration occurs at dislocation nodes, and atoms there are in high-energy, unstable states. Small tensile strain exists in the coherent regions that occupy most of the interface area. To characterize the degree of strain inhomogeneity near the interface, we define a strain inhomogeneity factor $K$, which is the absolute value of the ratio of the in-plane atomic strain $\bar{\varepsilon}$ to the average strain in the whole metal slab $\bar{\varepsilon}_{ave}$ ($K = |\bar{\varepsilon}/\bar{\varepsilon}_{ave}|$). Based on the above analysis, $K$ takes the maximum value at the node regions ($K_{max} = 1163.0$). When system energy increases under external loadings, atoms there have the greatest possibility to transform to a more stable atomic structure.

It is worth noting that the amplitude of strain fluctuation within one atomic monolayer decreases rapidly with increasing distance away from the interface, and the maximum strain fluctuation is in the first Ag ML. Similarly, elasticity theory estimated the induced strain field at interface varies as $h^{-1}$ for $h \ll \Lambda$ and as hexp(-h) for $h > \Lambda$ (h is the film thickness, $\Lambda$ is the period of interfacial dislocation network) in the vicinity of the dislocation core [37,38]. Although the residual strain is only distributed within a few nanometers of the interface, the complex atomic structure in this region, as well as the induced strain inhomogeneity, greatly influences the adhesion, mechanical strength and fracture behavior of metal/ceramic interfaces.

### 3.2. Interface energy and work of adhesion

Interface energy depends on both interface chemical components and atomic structure [39], and it reflects the stability of the interface. From the above relaxed interface structure, the equilibrium interface distance ($d_{int}$) and interface energy ($\gamma_{int}$) can be obtained. $d_{int}$ is the average distance between interfacial Ag ML and MgO ML. $\gamma_{int}$ is calculated as the superabundance energy relative to the bulk materials due to the existence of interface [40]:

$$\gamma_{int} = \frac{1}{S}\left[\sum_{l}^{l_{Ag}} (E_{Ag}^{l} - E_{Ag}^{b}) + \sum_{l}^{l_{MgO}} (E_{MgO}^{l} - E_{MgO}^{b})\right] \quad (4)$$

where $E_{Ag}^{l}$ and $E_{MgO}^{l}$ are the energies of the $l^{th}$ layer in the silver and magnesia slabs, $E_{Ag}^{b}$ and $E_{MgO}^{b}$ are the bulk energies of silver and magnesia, and $l_{Ag}$ and $l_{MgO}$ are the numbers of silver and magnesia monolayers in the interfacial region. Table 1 lists the calculated results. For comparison, the results of ideal Ag/MgO interface are also listed. It shows that the equilibrium interface distance of coherent interface is

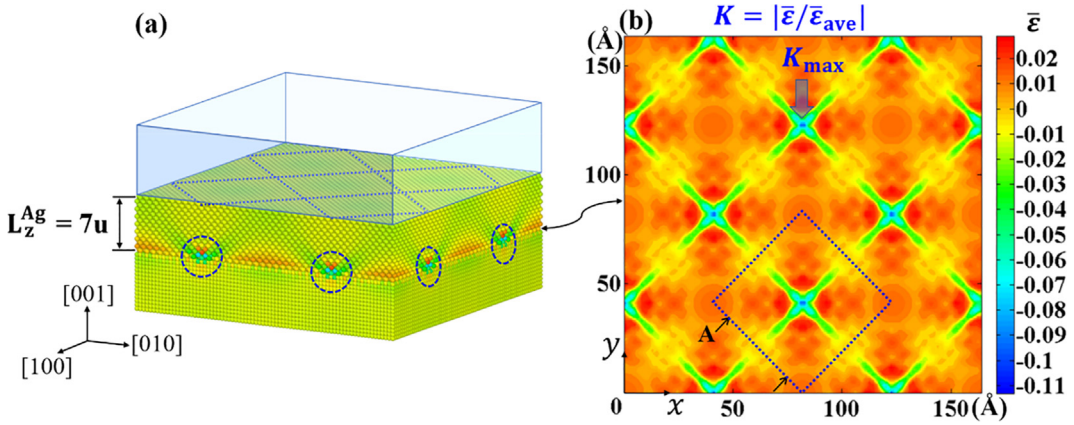


**Fig. 2.** (a) In-plane strain field near the Ag/MgO interface. For clarity, only 7 unit lattices in the Ag slab are shown and the dashed blue circles mark the dislocation nodes and the dashed lines mark the location of MDN at the interface. (b) The distribution of atomic strain in the first Ag ML adjacent to the Ag/MgO interface. At dislocation nodes, the strain inhomogeneity ($K$) is the maximum.

**Table 1**
Some fundamental interface quantities for both coherent and semi-coherent Ag/MgO interfaces. $d_{int}$: equilibrium interface distance. $\gamma_{int}$: interface energy.$W_{ad}$: work of adhesion.

| | $d_{int}$ (Å) | | | $\gamma_{int}$ (J/m$^2$) | | | $W_{ad}$ (J/m$^2$) | | |
|---|---|---|---|---|---|---|---|---|---|
| | This work | *Ab initio* | Experiment | This work | Theory | Experiment | This work | *Ab initio* | Experiment |
| Coherent interface | 2.38 | 2.34 [41]<br>2.38 [42] | 2.52 ± 0.1 [10]<br>2.52 [29] | 3.50 | – | 2.24 ± 0.1 [29] | 0.99 | 0.80 [43]<br>0.95 [44] | 0.49–0.89 [45]<br>0.45 ± 1 [29] |
| Semi-coherent interface | 2.44 | – | | 3.94 | 3 [39] | | 0.62 | < 0.5 [44] | |

2.38 Å, which is consistent with *ab initio* calculation results [41,42]. Due to the existence of MDN, $d_{int}$ of semi-coherent interface is slightly larger (2.44 Å), which is within the range of experimental results at room temperature [10]. Besides, interface energy of semi-coherent interface is higher than that of coherent interface, implying more unstable interface and easier interface separation. The existence of misfit dislocations causes lattice distortion in the interfacial region, correspondingly, the atomic energies in this region increase. Based on the difference in $\gamma_{int}$ between coherent and semi-coherent interfaces, the misfit dislocation energy is estimated to be 0.44 J/m$^2$, a little higher than the dislocation energy of Ag/MgO interface without dislocation nodes (≈0.32 J/m$^2$ [24]).

Work of adhesion ($W_{ad}$) is a measure of interface bond strength. As the reversible work needed to separate an interface into two free surfaces, $W_{ad}$ can be obtained by subtraction of total energies at equilibrium from slab energies at large interface separation [46]:

$$W_{ad} = \frac{E_{Ag}^{slab} + E_{MgO}^{slab} - E_{tot}}{S} \tag{5}$$

where $E_{Ag}^{slab}$ and $E_{MgO}^{slab}$ are the energies of isolated Ag slab and MgO slab, $E_{tot}$ is the total energy of the equilibrium Ag/MgO interface system, and $S$ is the interface area. The existence of misfit dislocations reduces the number of Ag-O bond that contributes to interface adhesion. Consequently, $W_{ad}$ of semi-coherent interface is nearly 40% lower than that of coherent interface, as shown in Table 1. Actually, an alternative expression of Eq. (5) is:

$$W_{ad} = \gamma_{Ag}^{surf} + \gamma_{MgO}^{surf} - \gamma_{int} \tag{6}$$

where $\gamma_{Ag}^{surf}$ and $\gamma_{MgO}^{surf}$ are the surface energies of Ag and MgO. Theoretically, the sum of $W_{ad}$ and $\gamma_{int}$ is a constant ($\gamma_{Ag}^{surf} + \gamma_{MgO}^{surf}$), which depends on the constituent materials of the interface system and the crystal orientation [47]. Note that in the equilibrium coherent and semi-coherent interface structures, the residual strains on Ag are not identical, which will result in small variation in $\gamma_{Ag}^{surf}$. Thus, the sums of $W_{ad}$ and $\gamma_{int}$ show minor differences.

## 4. Results of interface shear

### 4.1. Interface constitutive relationship

To explore the interface shear constitutive relationship, shear loading is applied along the direction of Burgers' vector ([1 1 0] crystal orientation), and the changes of interface traction $T_t$ are recorded. The thickness of metal slab ($L_z^{Ag}$) and ceramic slab ($L_z^{MgO}$) are both 10 unit lattices, denoted by 10u-10u.

Fig. 3(a) shows the periodic variation of interface traction $T_t$ during interface shear process and Fig. 3(b) shows the corresponding interface atomic configurations. In the first period (point A to point B), $T_t$ increases linearly with the increase of $\delta_t$ until the interface strength (0.40 GPa). Then with the jump of Ag slab, $T_t$ decreases by 0.15 GPa and the second loading period begins. At point B, Ag slab slips by approximately 0.2 Å relative to the MgO slab, and part of the elastic strain energy is released with recovery of bending dislocations.

Fig. 3(b) also shows the distribution of atomic potential energies (PE). It is clear that the atomic potential energies are higher at the dislocation nodes and the middle of dislocation lines between two nodes (point A). With increasing loading displacement, those high-energy atoms between nodes move first and the dislocation lines bend toward the shear direction (point B). Then at the critical point B, nodes jump by |a/2[110]| to the next stable positions and the atomic energies near the dislocation lines decrease (point C). This node jump leads to the sudden drop of $T_t$ in Fig. 3(a). As the second period begins, dislocation lines bend again (point D). From the above analysis, it can be concluded that dislocation nodes serve as strong pinning points to the gliding motion of MDN. Therefore, for Ag/MgO interface with MDN, the shear strength is increased compared with the one-dimensional semi-coherent Ag/MgO interface without nodes [27], though it is still much lower than the ideal strength of coherent interface. Besides, interface shear is accompanied by periodic variations of atomic energy near the interface.

The area under the $T_t - \delta_t$ curve in Fig. 3(a) represents the cohesive work $W_{coh}$ for interface slip, which is different from the work of adhesion ($W_{ad}$) in normal direction. In the first period $W_{coh1}$ is calculated to be 0.0046 J/m$^2$ and in the second period $W_{coh2}$ is a little smaller (0.0032 J/m$^2$). The difference in $W_{coh}$ is caused by the stored elastic strain energy in bulk materials at point C. Besides, $W_{coh1}$ and $W_{coh2}$ are two orders of magnitude smaller than those of coherent interface ($W_{coh1}$ = 0.30 J/m$^2$, $W_{coh2}$ = 0.25 J/m$^2$ [27]), while in normal direction the decrease in $W_{ad}$ from coherent to semi-coherent interface is only about 40%, as discussed in Section 3.2. This obvious contrast implies that MDN greatly increases the possibility of shear failure rather than tensile failure at the Ag/MgO interface.

### 4.2. Energy analysis

The energy criterion for interface fracture has always been the subject of interface research [4,41,48]. To understand the role of misfit dislocation in interface shear process further, related energy variations are analyzed.

For semi-coherent Ag/MgO interface with MDN, the total energy ($E_{tot}$) can be regarded as the summation of several energy terms, namely the bulk energy, surface energy ($\gamma_{Ag}^{surf}$, $\gamma_{MgO}^{surf}$) and interface energy ($\gamma_{int}$). The $\gamma_{int}$ of semi-coherent interface can be further viewed as the sum of coherent interface energy $\gamma_{int}^{cohe}$ and misfit dislocation energy $E_{dis}$. In the shear process the change of total energy is mainly reflected by the change of elastic strain energy stored in bulk materials and the change of interface energy, which is closely associated with the motion of MDN. By subtracting the above energy contributions from the total energy of semi-coherent Ag/MgO interface system, the misfit dislocation energy $E_{dis}$ in the shear process can be expressed as:

$$E_{dis} = \frac{E_{tot} - n_{Ag}\alpha_{Ag} - n_{MgO}\alpha_{MgO}}{S} - (\gamma_{Ag}^{surf} + \gamma_{MgO}^{surf} + \gamma_{int}^{cohe}) \tag{7}$$

where $E_{tot}$ denotes the total energy of the interface system, $n_{Ag}$ and $n_{MgO}$ are the numbers of atoms in Ag slab and MgO slab, and $S$ is the interface area. $\alpha_{Ag}$ and $\alpha_{MgO}$ denote the lattice energy. Unlike conventional lattice energy as a material parameter, $\alpha_{Ag}$ and $\alpha_{MgO}$ here vary with the elastic deformation of the bulk materials. Therefore, $\Delta\alpha_{Ag}$ and $\Delta\alpha_{MgO}$ represent the variation of elastic strain energy. $\Delta E_{tot}$ and $\Delta E_{dis}$ represent the variations of total energy and dislocation energy, respectively. $\gamma_{Ag}^{surf}$ and

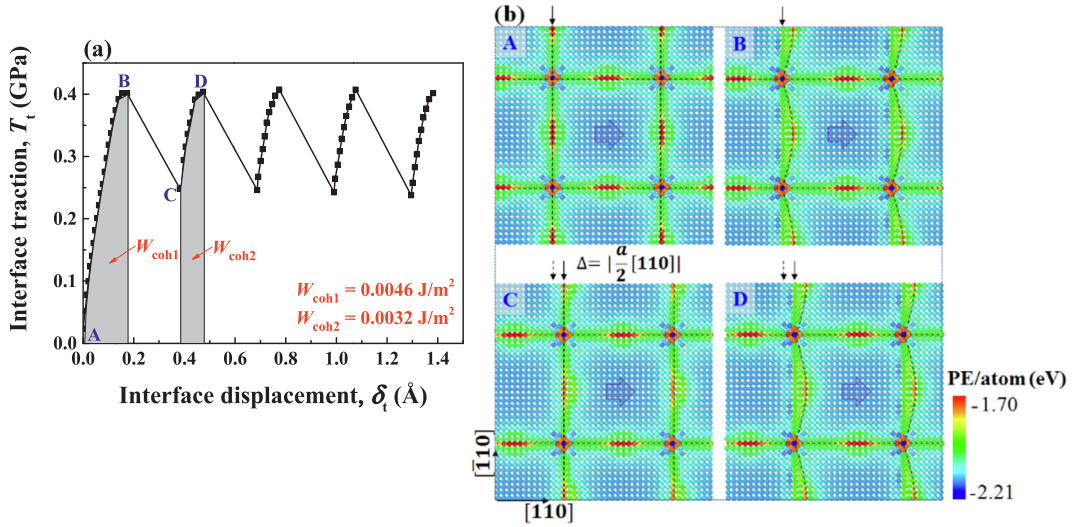


**Fig. 3.** (a) The shear traction-displacement relationship of Ag/MgO interface system (10u-10u). (b) The interface atomic configurations corresponding to key points A-D in (a). For clarity, only the first Ag ML adjacent to the interface is shown and atoms are colored in accordance with their potential energies (PE).

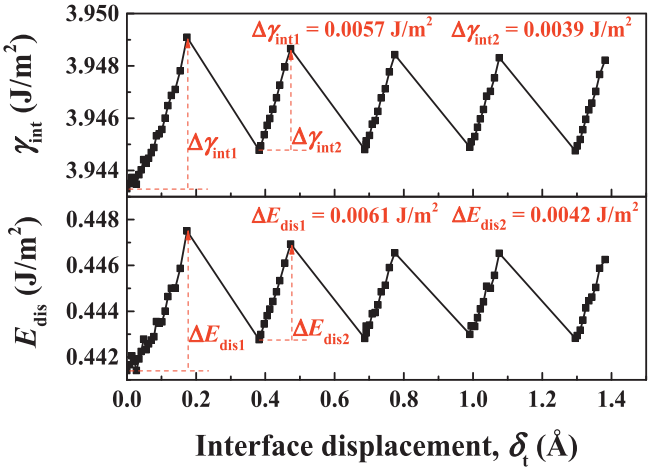


**Fig. 4.** The variation of interface energy $\gamma_{int}$ and dislocation energy $E_{dis}$ in the shear process of Ag/MgO interface.

$\gamma_{MgO}^{surf}$ denote the unit-area surface energies (their changes can be neglected here) and $\gamma_{int}^{cohe}$ is the unit-area interface energy for ideal coherent interface. Except for $\gamma_{int}^{cohe}$, all energies are obtained directly from the relaxed semi-coherent Ag/MgO interface system. Note that both interface energy $\gamma_{int}$ based on Eq. (4) and misfit dislocation energy $E_{dis}$ based on Eq. (7) change periodically during interface shearing. Fig. 4 shows the comparison between calculated $\gamma_{int}$ and $E_{dis}$ of the 10u-10u Ag/MgO interface model.

It can be seen that the trends of the two curves are basically the same. Although the value of dislocation energy is only about one-tenth of the interface energy, the change of dislocation energy ($\Delta E_{dis}$) during shearing is almost equal to that of interface energy ($\Delta\gamma_{int}$). At first, $\gamma_{int}$ and $E_{dis}$ increase as the interface displacement $\delta_t$ increases, which corresponds to the bending of dislocation lines. Then misfit dislocations move over the "hills" – the energy barrier ($\Delta E_{dis}$) – and reach the next stable positions, which corresponds to the jump of dislocation nodes and the decrease of $\gamma_{int}$ and $E_{dis}$. After that, the entire MDN moves along the shear direction by the length of Burgers vector (|a/2[110]|). As the second loading period begins, $\gamma_{int}$ and $E_{dis}$ increase again. From Fig. 4, the average energy barriers $\Delta E_{dis}$ in the first and the second period are ≈0.0059 J/m$^2$ and ≈0.0041 J/m$^2$, respectively.

According to the definition of Peierls stress [49], the energy barrier is the integral of shear stress:

$$\int \tau d\delta_t = \Delta E_{dis} \quad (8)$$

where $\tau$ is the shear stress. Comparing with Fig. 3(a), the energy barriers $\Delta E_{dis}$ are roughly consistent with the cohesive work $W_{coh}$ ($W_{coh1}$ = 0.0046 J/m$^2$, $W_{coh2}$ = 0.0032 J/m$^2$). This indicates that the shear strength of Ag/MgO interface is largely dependent on the variation of misfit dislocation energy.

### 4.3. Effect of model thickness

In order to explore the effect of model thickness, the lattice numbers of Ag and MgO along the thickness direction remain the same ($L_z^{Ag} = L_z^{MgO}$) and $L_z$ varies from 10u to 20u.

Fig. 5(a) shows the traction – displacement relationship during the shear process. For thin model (10u–10u), interface traction $T_t$ changes periodically and the interface shear strength is 0.4 GPa, which is close to the interface shear strengths of other metal/ceramic interfaces, such as the MD simulation result of Ti/TiN interface (0.38 GPa) [23] and experimental result of Al-$MgAl_2O_4$ interface at ambient temperature (0.82 ± 0.18 GPa) [48]. As the model thickness increases (15u–15u, 20u–20u), more elastic strain energy is stored in the interface system, and it shows that the shear traction is unstable, which eventually decreases to ≈0.3 GPa. In-situ compression testing of CrN/Cu/Si(1 0 0) micro-pillars also reported the shear strength decreases as the Cu interlayer thickness increases [23,25]. Dislocation theory has been successfully used to explain the thickness effect of some metal/metal multilayers containing plastic deformation [50]. Our simulation results also suggest that the transformation of dislocation structure (Fig. 5(b)) contributes to the decrease in shear strength.

Fig. 5(b) shows the interfacial atomic configurations corresponding to the marked points B′-E′ in Fig. 5(a) (20u–20u model). In the first period, the motion characteristics of MDN are almost the same for different thickness models, and hence the shear strengths at point B′ are identical. After the first jump of dislocation nodes (point C′), the atomic structure of one node (marked by the circle) transforms to a more energetically favoured configuration. The dislocation line around this "special" node splits. During the second period of loading, the split dislocation lines bend in a much smaller degree (point D′), which suggests that the pinning effect of this node is weakened. After the second jump of dislocation nodes (point E′), more nodes undergo structural transformation, which ultimately leads to decrease in $T_t$ (Fig. 5(a)) and increase in $\delta_n$ as shown in Fig. 6. Similar change in the node structure under mechanical shear has been reported in molecular

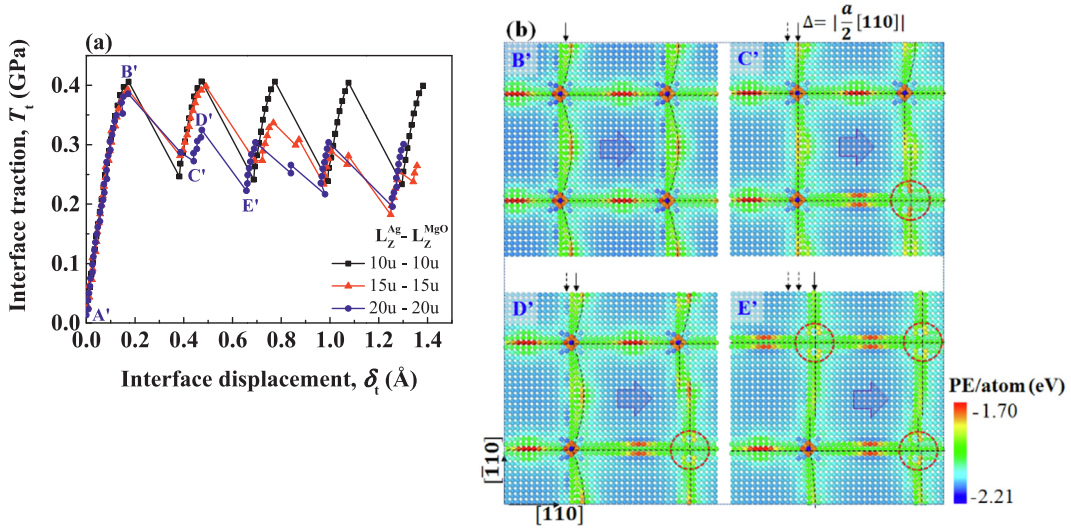


**Fig. 5.** (a) The shear traction-displacement relationships of Ag/MgO interface systems with different thicknesses. (b) The transformation of dislocation structure during the shear process (20u–20u model). Graphs B′-E′ correspond to the points B′-E′ marked in (a). Only the first Ag ML adjacent to the interface is shown and atoms are colored in accordance with their potential energies (PE).

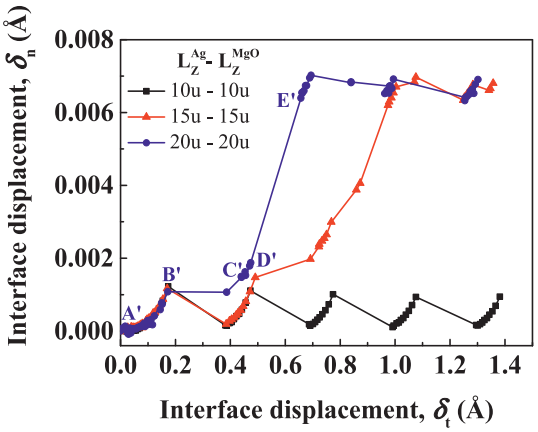


**Fig. 6.** The changes of interface distance during shearing of Ag/MgO interface systems with different thicknesses.

static/dynamics simulations of semi-cohernet Cu(1 1 1)/Ni(1 1 1) interface [51].

As mentioned in Section 4.2, the shear strength of Ag/MgO interface mainly depends on the variation of dislocation energy $\Delta E_{dis}$. After the node structure changes in the second period, $\Delta E_{dis}$ of the 20u-20u interface model (0.0030 J/m$^2$) decreases obviously compared with that of the first period (0.0055 J/m$^2$, see Fig. S1 in Supplementary Materials, while $\Delta E_{dis}$of 10u-10u and 15u-15u interface models have nearly no change, so the interface shear strength of 20u-20u model decreases based on Eq. (8). As more nodes transform to the energetically favored strucure, interface shear strength converges to nearly 0.3 GPa. What's more, theoretical research based on the interface thermodynamics also showed that interface energy and dislocation energy increased with increasing model thickness, and when the model thickness was larger than 12 nm this size effect was not significant [39]. In initial equilibrium interface models, the dislocation energy $E_{dis}$ of 15u–15u and 20u-20u interface models are 0.454 J/m$^2$ and 0.455 J/m$^2$, respectively, while $E_{dis}$ of the 10u-10u interface model is 0.442 J/m$^2$ (Fig. S1). Higher $E_{dis}$ indicates more unstable misfit dislocation structure. Therefore, thick model (20u–20u) is more prone to change node structure.

Fig. 6 shows the variation of interface distance, i.e., interface normal displacement $\delta_n$. Equilibrium interface distance is taken as the reference. In general, dislocation motion in the shear direction is coupled with tiny changes in interface distance in the normal direction. For thin model (10u–10u), $\delta_n$ increases slightly before dislocation nodes jump to the next stable positions. After the movement of dislocation nodes, interface distance returns to its equilibrium value. For thick models (15u–15u, 20u–20u), one can see obvious increase in $\delta_n$ after several periods, which also implies that thick model is easier to lose stability. Although the change in interface distance is rather small (less than 0.01 Å), the corresponding traction drop is large (≈0.1 GPa).

Similar to the energy analysis in Section 4.2, Table 2 lists the energy barriers in the first two periods for Ag/MgO interface systems with different thicknesses. The maximum strain inhomogeneity factor $K_{max}$ at the critical point B' are also listed and the corresponding distributions of $\bar{\varepsilon}/\bar{\varepsilon}_{ave}$ are shown in Fig. 7.

In the first period, the interface cohesive work $W_{coh1}$ is almost the same for different models, while the energy barrier $\Delta E_{tot1}$ increases proportionally with the increase of model thickness, which indicates more elastic strain energy is stored in thick models. Correspondingly, the ratio of $W_{coh1}$ to $\Delta E_{tot1}$ decreases with increasing thickness. In the second period, both $W_{coh2}$ and $\Delta E_{tot2}$ are smaller than the values in the first period, and different models show different energy variations.

For thin models (10u–10u, 15u–15u), the energy barriers of interface shear are ≈0.01 J/m$^2$ and the ratios $W_{coh2}/\Delta E_{tot2}$ are ≈0.35, which is bigger than the values in the first period. These results suggest that in

**Table 2**
The interface cohesive work and energy barriers in the first two periods for Ag/MgO interface systems with different thicknesses. $K_{max}$: the maximum strain inhomogeneity factor at the critical point B' in Fig. 5.

| $L_z^{Ag} - L_z^{MgO}$ | $W_{coh1}$ (J/m$^2$) | $\Delta E_{tot1}$ (J/m$^2$) | $W_{coh2}$ (J/m$^2$) | $\Delta E_{tot2}$ (J/m$^2$) | $W_{coh1}/\Delta E_{tot1}$ | $W_{coh2}/\Delta E_{tot2}$ | $K_{max}$ (point B′) |
|---|---|---|---|---|---|---|---|
| 10u–10u | 0.00437 | 0.0138 | 0.00316 | 0.00908 | 0.317 | 0.348 | 1317.5 |
| 15u–15u | 0.00406 | 0.0170 | 0.00371 | 0.0102 | 0.239 | 0.364 | 1933.7 |
| 20u–20u | 0.00419 | 0.0209 | 0.000998 | 0.00466 | 0.200 | 0.214 | 2549.0 |

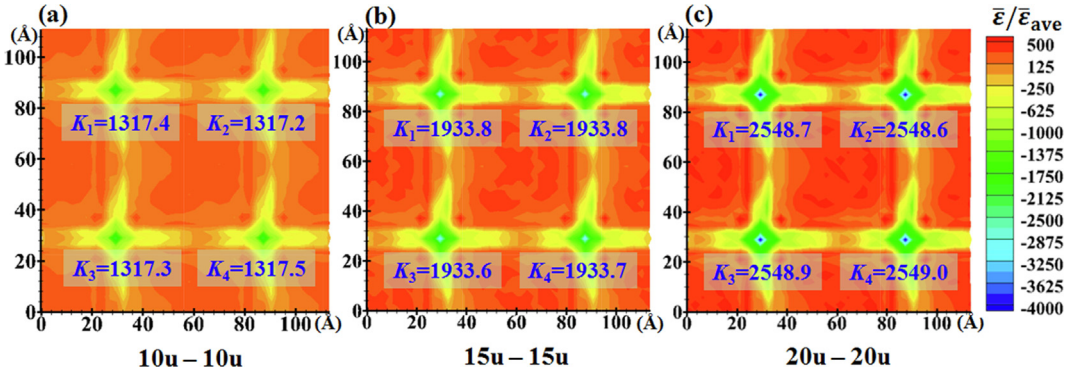


**Fig. 7.** The strain inhomogeneity in the interfacial Ag ML for Ag/MgO interface systems with different thicknesses (at the critical point B' in Fig. 5(a)). The values of strain inhomogeneity factor $K$ at dislocation nodes are marked. (a) 10u–10u model. (b) 15u–15u model. (c) 20u–20u model.

the second period of shear loading, a greater proportion of the total energy is consumed in interface slipping and the elastic deformation of the bulk materials is reduced. For thick model (20u–20u), due to the transformation of nodal structure, both $W_{coh2}$ and $\Delta E_{tot2}$ are about an order of magnitude smaller than the values of the other two models. Besides, the ratio $W_{coh2}/\Delta E_{tot2}$ also goes down. It is evident that, to some extent, the thicker the interface model, the worse the interface adhesive property during interface slip.

It is clearly demonstrated in Fig. 7 that for interface models with different thicknesses, the strain inhomogeneity at the dislocation region increases significantly. In this region, the in-plane strain $\bar{\varepsilon}$ near the dislocation line is larger and it reaches the maximum at the node regions. With the increase of model thickness, the strain concentration at the node regions becomes more severe (1317.5 → 2549.0), which explains, from a different perspective, why the dislocation structure of thick model is more prone to transform. Note that the value of $K$ at the fourth node ($K_4$ in Fig. 7(c)) is the largest, correspondingly, this node is the first to undergo structural transformation. In fact, Fig. 7 shows the overall effect of in-plane strain which is the superposition of internal strain caused by MDN and strain caused by externally applied shear loading. In interface dynamics, the strain/stress concentration regions are "dangerous" regions.

Note that the thickness ratio between metal and ceramic also influences the mechanical response of metal/ceramic multilayers [18,21]. Next, we investigate the thickness ratio effect by varying the thickness of Ag layer and MgO layer while keeping the total thickness of the interface structure a constant.

Fig. 8(a) shows the interface shear constitutive relationships of Ag/MgO interfaces with different thickness ratios. For the interface model with thicker Ag layer (18u–12u), interface shear strength decreases after the first period due to the transformation of dislocation structure, and $\Delta E_{dis}$ in the second period is smaller compared with $\Delta E_{dis}$ of the other two models (Fig. 8(b)). On one hand, more elastic strain energy is stored in the thicker metal layer at the critical point (the first peak stress $T_t$), and the change of dislocation structure can release some elastic strain energy. On the other hand, the lattice distortion caused by MDN is mainly distributed in the softer metal side, so the misfit dislocation energy $E_{dis}$ increases with the increase of metal layer thickness within the thickness range here (Fig. 8(b)) and the corresponding interface structure is more unstable, especially in the high energy dislocation node regions where strain concentration occurs. In interface dynamic shearing process, the combined effect of elastic strain energy and dislocation energy results in the structural transformation of some dislocation nodes, which affects the interface mechanical properties significantly [51].

In short, the simulation results of Ag/MgO interface models with different thicknesses and different thickness ratios all show that the interfacial shear strength decreases with increasing model thickness, especially metal layer thickness.

### 4.4. Effect of shear direction

In practical applications, shear loadings may be applied in any direction, thus interface shear along different directions are investigated. First, let's deduce the relationship between shear stress and shear direction. Assume the angle between the shear direction and the dislocation line is $\alpha$ degrees. Considering the symmetry of MDN, $\alpha$ is in the range of 0° to 90°. For the gliding motion of MDN, if the critical force required to surmount the energy barrier along the direction of Burgers vector is $F_I$, then according to the parallelogram rule, the critical force $F$ along any direction should be:

$$F = F_I \times (\sin\alpha + \cos\alpha) = \sqrt{2} F_I \times \sin(\alpha + 45°) \quad (9)$$

or

$$F/F_I = \sqrt{2} \times \sin(\alpha + 45°), (0° \le \alpha < 90°) \quad (10)$$

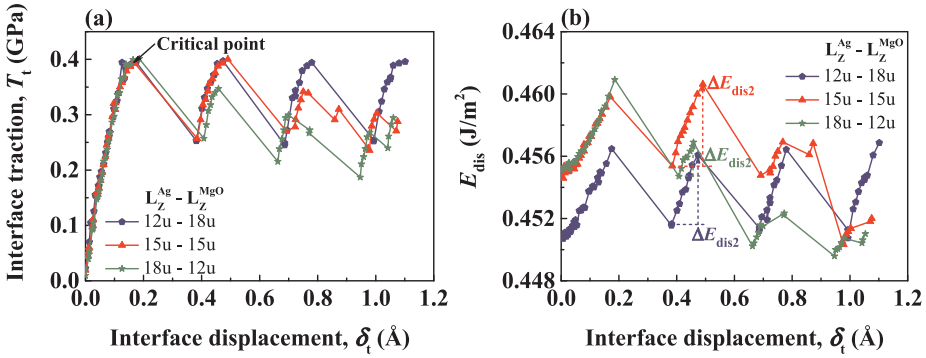


**Fig. 8.** (a) The shear traction-displacement relationships of Ag/MgO interface systems with different thickness ratios. (b) The variations of dislocation energies $E_{dis}$ during shearing of Ag/MgO interface systems with different thickness ratios.

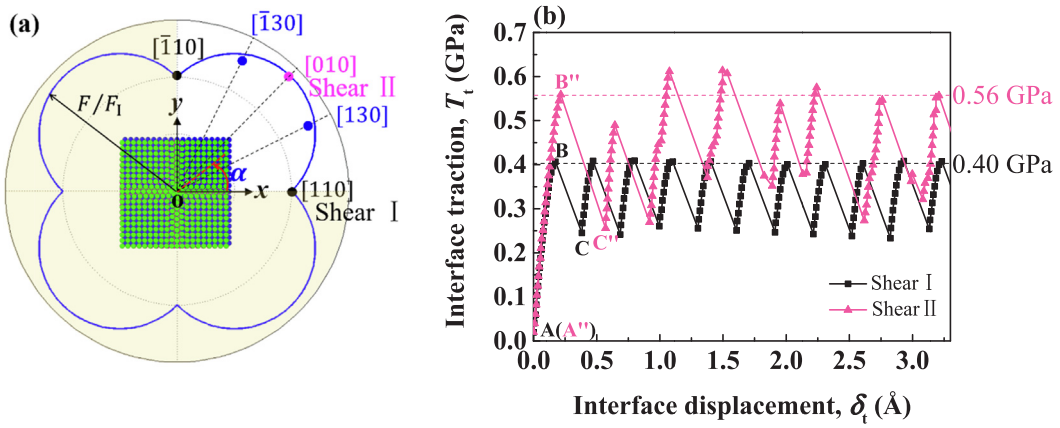


**Fig. 9.** (a) The relationship between interface shear strength and shear direction (blue curve). The points represent the simulated results of shear strengths along three different directions. (b) Interface shear traction – displacement relationships for Ag/MgO interfaces shearing along the directions [1 1 0] (Shear I) and [0 1 0] (Shear II).

Fig. 9(a) draws this relationship (blue curve) and the distance from a point on the curve to the origin represents the dimensionless shear strength along that direction, $F/F_I$. It can be seen that $\alpha = 45^\circ$ corresponds to the maximum strength, and when the shear direction is parallel to one set of misfit dislocation arrays ($\alpha = 0^\circ$), strength $F$ is the minimum. In order to check Eq. (10), interface shear simulations along three directions ($\alpha = 0^\circ$, $\alpha = 26.5^\circ$ and $\alpha = 45^\circ$) are conducted, and the points in Fig. 9(a) represent the simulated results of $F/F_I$. It shows that the calculated shear strengths agree well with the prediction of Eq. (10).

The interface shear traction – displacement relationships along two typical shear directions (Shear I and Shear II) are shown in Fig. 9(b). Compared with Shear I, in Shear II both the shear strength and the change of $T_t$ over one period are larger. Moreover, shear strength fluctuates in accordance with the gliding motion of MDN along the [0 1 0] direction. The averaged shear strength in Shear II is 0.56 GPa, and the shear strength in Shear I is 0.40 GPa, which is consistent with the prediction of Eq. (10) (0.56 GPa/0.40 GPa$\approx\sqrt{2}$). In summary, the property of interface shear along different directions depends largely on the geometry of MDN, and the shear strength along the direction of Burgers vector is the lowest. In fact, this conclusion is common for other interfaces with MDN [52,53].

Next, we focus on the gliding motion of MDN along the above two typical directions. The in-plane atomic displacements corresponding to the key points B(B″) and C(C″) in Fig. 9(b) are shown in Fig. 10.

The motion of MDN along [1 1 0] and [0 1 0] directions show similar characteristics: the atomic displacements are spatially non-uniform during interface shear process, which can be divided into two stages. In the first stage, all atoms in the first Ag ML move slightly and atoms between nodes have longer slip distance, with slip directions deviating from the applied shear direction (Fig. 10(a) and (c)). In the second stage, atoms in the node regions exhibit the longest slip distance (Fig. 10(b) and (d)). Besides, MDN glides by the length of Burgers vector ($\Delta_I$) along the applied shear direction in Shear I, and in Shear II MDN glides by a relatively longer distance $\Delta_{II}$. In fact, interface displacements along different directions also turn out to obey a similar rule as Eq. (10).

To be brief, nodes have strong pinning effects to the gliding motion of MDN. In dislocation line regions the shear resistance is relatively low, while in dislocation node regions the shear resistance is high, reflected by the small atomic displacements at point B(B″). In addition, along the direction of Burgers vector MDN glides by the shortest distance in one period, which explains the periodic interface displacement in Shear II is larger than that in Shear I, as shown in Fig. 9(b).

## 5. Conclusions

In this work, atomistic simulations have been performed to explore the static and dynamic characteristics of Ag/MgO interface with MDN.

Firstly, in-plane strain analysis demonstrates that the local strain induced by MDN varies in a periodic pattern, with significant strain concentration at the node regions. At several atomic layers away from the interface the strain field is reversed, implying complex strain distribution within the small interfacial region. This weakens the interface adhesion, which is also verified by the reduced work of adhesion and increased interface energy compared with ideal interface.

The gliding motion of MDN is found to be dominant in the shear process of semi-coherent Ag/MgO interface. With the motion of MDN, interface shear traction changes periodically and the shear stress is determined mainly by the variation of misfit dislocation energy. Nodes serve as strong pinning points to the motion of MDN, and noticeable bending of disocation lines occurs before nodes jump to the next stable positions. After the jump of nodes, MDN slips by the length of Burgers vector along the shear direction.

When model thickness or thickness ratio between Ag layer and MgO layer increases, both interface shear strength and dislocation energy barriers decrease. This is because more elastic strain energy is stored in bulk materials, the strain inhomogeneity near the interfce is more significant as well, so the interface structure is unstable during the shear process – nodes transform to a more energetically preferred structure. This suggests that the thicker the model thickness, the more pronounced the “weak link” characteristic of the interface.

For interface shear along different diretions, the geometrical feature of MDN largely determines the interface shear characteristics, and both the shear strength and gliding distance of MDN turn out to obey the same relationship. Besides, Ag/MgO interface has the greatest possibility to undergo shear failure along the direction of Burgers vector.

The results in this paper provide some insight into understanding the crucial role of MDN in interface shear process, and the conclusions can be extended to other similar metal/ceramic interfaces. Temperature and strain rate are also of much concern in metal/ceramic interface research, and further work about their influences will be carried out.

## CRediT authorship contribution statement

**X.Q. Fu:** Data curation, Software, Investigation, Writing - original draft. **L.H. Liang:** Conceptualization, Methodology, Formal analysis, Funding acquisition, Writing - review & editing. **Y.G. Wei:** Conceptualization, Methodology, Funding acquisition.

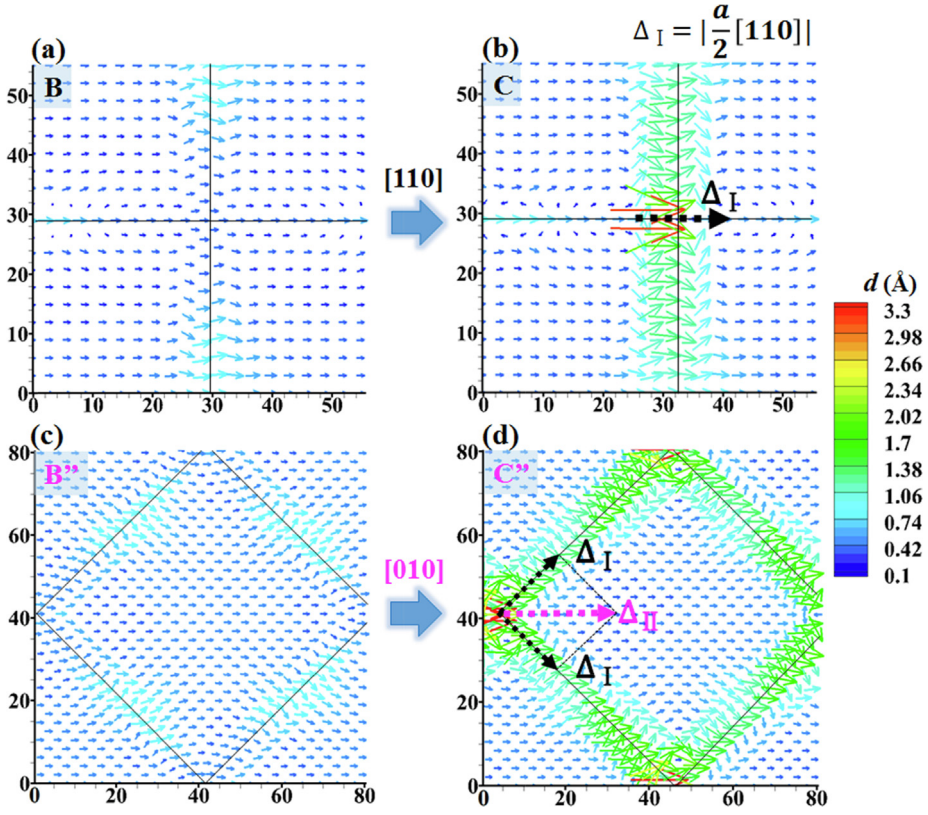


**Fig. 10.** The distribution of in-plane atomic displacements in the interfacial Ag ML corresponding to the key points B(B″) and C(C″) in Fig. 9(b). $\Delta_I$ and $\Delta_{II}$: the gliding distance of MDN in one period. (a) and (b): along the [1 1 0] direction (Shear I). (c) and (d): along the [0 1 0] direction (Shear II). The equilibrium interface structure is taken as the reference.


## Acknowledgments

This work was financially supported by the National Natural Science Foundation of China (Nos. 11672296, 91860102, 11432014, 11672301, 11890681) and the Strategic Priority Research Program of the Chinese Academy of Sciences (Grant No. XDB22040501).


## Data availability

The raw/processed data required to reproduce these findings cannot be shared at this time due to technical or time limitations.

## Appendix A. Supplementary data

Supplementary data to this article can be found online at https://doi.org/10.1016/j.commatsci.2019.109151.

## References


[1] M.W. Finnis, The theory of metal – ceramic interfaces, J. Phys.: Condens. Matter 8 (1996) 5811–5836, https://doi.org/10.1088/0953-8984/8/32/003.

[2] X.G. Wang, J.R. Smith, A. Evans, Fundamental influence of C on adhesion of the Al2O3/Al interface, Phys. Rev. Lett. 89 (28) (2002) 286102–286106, https://doi.org/10.1103/PhysRevLett. 89.286102.

[3] Z. Zhang, Y. Long, S. Cazottes, R. Daniel, C. Mitterer, G. Dehm, The peculiarity of the metal-ceramic interface, Sci. Rep. 5 (2015) 11460, https://doi.org/10.1038/srep11460.

[4] M. Kwan, M. Braccini, A. Jain, M.W. Lane, G. Ramanath, Interplay between bond breaking and plasticity during fracture at a nanomolecularly-modified metal-ceramic interface, Scr. Mater. 121 (2016) 42–44, https://doi.org/10.1016/j.scriptamat.2016.04.034.

[5] D.A. Snelling, C.B. Williams, C.T.A. Suchicital, A.P. Druschitz, Binder jetting advanced ceramics for metal-ceramic composite structures, Int. J. Adv. Manuf. Technol. 92 (1–4) (2017) 531–545, https://doi.org/10.1007/s00170-017-0139-y.

[6] A. Kumar, H. Barda, L. Klinger, M.W. Finnis, V. Lordi, E. Rabkin, D.J. Srolovitz, Anomalous diffusion along metal/ceramic interfaces, Nat. Commun. 9 (2018) 1–8, https://doi.org/10.1038/s41467-018-07724-7.

[7] V. Vitek, G. Gutekunst, J. Mayer, M. Rühle, Atomic structure of misfit dislocations in metal-ceramic interfaces, Philos. Mag. A 71 (6) (1995) 1219–1239, https://doi.org/10.1080/01418619508244370.

[8] R. Benedek, A. Alavi, D.N. Seidman, L.H. Yand, D.A. Muller, C. Woodward, First principles simulation of a ceramic/metal interface with misfit, Phys. Rev. Lett. 84 (15) (2000) 3362–3365, https://doi.org/10.1103/PhysRevLett. 84.3362.

[9] P. Guenard, G. Renaud, B. Villette, Structure, translational state and morphology of the Ag/MgO(001) interface during its formation, Physica B 221 (1996) 205–209, https://doi.org/10.1016/0921-4526(95)00925-6.

[10] O. Robach, G. Renaud, A. Barbier, Structure and morphology of the Ag/MgO(001) interface during in situ growth at room temperature, Phys. Rev. B 60 (8) (1999) 5858–5871, https://doi.org/10.1103/PhysRevB.60.5858.

[11] H. Meltzman, D. Mordehai, W.D. Kaplan, Solid–solid interface reconstruction at equilibrated Ni–Al2O3 interfaces, Acta Mater. 60 (11) (2012) 4359–4369, https://doi.org/10.1016/j.actamat.2012.04.037.

[12] S.V. Kamat, J.P. Hirth, Dislocation injection in strained multilayer structures, J. Appl. Phys. 67 (11) (1990) 6844–6850, https://doi.org/10.1063/1.345074.

[13] J.R. Willis, S.C. Jain, R. Bullough, The energy of an array of dislocations, Philos. Mag. A 64 (3) (1991) 629–640, https://doi.org/10.1080/01418619108204865.

[14] Y.G. Yao, T.C. Wang, C.Y. Wang, Peierls-Nabarro model of interfacial misfit dislocation: an analytic solution, Phys. Rev. B 59 (12) (1999) 8232–8236, https://doi.org/10.1103/PhysRevB.59.8232.

[15] G.E. Beltz, L.B. Freund, Analysis of the strained-layer critical thickness concept based on a Peierls—Nabarro model of a threading dislocation, Philos. Mag. A 69 (1) (2006) 183–202, https://doi.org/10.1080/01418619408242217.

[16] B.J. Lee, M.I. Baskes, Second nearest-neighbor modified embedded-atom-method potential, Phys. Rev. B 62 (13) (2000) 8564–8567, https://doi.org/10.1103/PhysRevB.62.8564.

[17] M. Damadam, S. Shao, G. Ayoub, H.M. Zbib, Recent advances in modeling of interfaces and mechanical behavior of multilayer metallic/ceramic composites, J. Mater. Sci. 53 (8) (2017) 5604–5617, https://doi.org/10.1007/s10853-017-1704-3.

[18] M. Damadam, S. Shao, I. Salehinia, G. Ayoub, H.M. Zbib, Molecular dynamics simulations of mechanical behavior in nanoscale ceramic–metallic multilayer composites, Mater. Res. Lett. 5 (5) (2017) 306–313, https://doi.org/10.1080/21663831.2016.1275864.

[19] Y. Long, N.X. Chen, W.Q. Zhang, Pair potentials for a metal–ceramic interface by inversion of adhesive energy, J. Phys.: Condens. Mat. 17 (12) (2005) 2045–2058, https://doi.org/10.1088/0953-8984/17/12/025.

[20] Y. Long, N.X. Chen, Pair potential approach for metal/Al2O3 interface, J. Phys.: Condens. Mat. 19(19) (2007) 196216, , https://doi.org/10.1088/0953-8984/19/

19/196216.
[21] I. Salehinia, J. Wang, D.F. Bahr, H.M. Zbib, Molecular dynamics simulations of plastic deformation in Nb/NbC multilayers, Int. J. Plast. 59 (2014) 119–132, https://doi.org/10.1016/j.ijplas.2014.03.010.
[22] S.K. Yadav, S. Shao, J. Wang, X.Y. Liu, Structural modifications due to interface chemistry at metal-nitride interfaces, Sci. Rep. 5 (2015) 17380, https://doi.org/10.1038/srep17380.
[23] X. Zhang, B. Zhang, Y. Mu, S. Shao, C.D. Wick, B.R. Ramachandran, W.J. Meng, Mechanical failure of metal/ceramic interfacial regions under shear loading, Acta Mater. 138 (2017) 224–236, https://doi.org/10.1016/j.actamat.2017.07.053.
[24] Y. Long, N.X. Chen, An atomistic simulation and phenomenological approach of misfit dislocation in metal/oxide interfaces, Surf. Sci. 602 (5) (2008) 1122–1130, https://doi.org/10.1016/j.susc.2008.01.018.
[25] Y. Mu, J.W. Hutchinson, W.J. Meng, Micro-pillar measurements of plasticity in confined Cu thin films, Extreme Mech. Lett. 1 (2014) 62–69, https://doi.org/10.1016/j.eml.2014.12.001.
[26] Y. Yao, Y. Zhang, Ab initio pair potentials at metal-ceramic interfaces, Phys. Lett. A 256 (1999) 391–398, https://doi.org/10.1016/S0375-9601(99)00263-7.
[27] X.Q. Fu, L.H. Liang, Y.G. Wei, Atomistic simulation study on the shear behavior of Ag/MgO interface, Comp. Mater. Sci. 155 (2018) 116–128, https://doi.org/10.1016/j.commatsci.2018.08.047.
[28] X.M. You, L.H. Liang, Y.G. Wei, The atomistic simulation study of Ag/MgO interface tension fracture, Comp. Mater. Sci. 142 (2018) 277–284, https://doi.org/10.1016/j.commatsci.2017.10.029.
[29] A. Trampert, F. Ernst, C.P. Flynn, H.F. Fischmeister, M. Ruhle, High-resolution transmission electron-microscopy studies of the Ag/MgO interface, Acta Metall. Mater. 40 (1992) S227–S236, https://doi.org/10.1016/0956-7151(92)90281-i.
[30] S. Plimpton, Fast parallel algorithms for short-range molecular dynamics, J. Comput. Phys. 117 (1) (1995) 1–19, https://doi.org/10.1006/jcph.1995.1039.
[31] A. Stukowski, Visualization and analysis of atomistic simulation data with OVITO–the open visualization tool, Modell. Simul. Mater. Sci. Eng. 18 (1) (2010) 015102, , https://doi.org/10.1088/0965-0393/18/1/015012.
[32] J.H. Irving, J.G. Kirkwood, The statistical mechanical theory of transport processes. IV. The equations of hydrodynamics, J. Chem. Phys. 18 (6) (1950) 817–829, https://doi.org/10.1063/1.1747782.
[33] K. Gall, M.F. Horstemeyer, M. Van Schilfgaarde, M.I. Baskes, Atomistic simulations on the tensile debonding of an aluminum-silicon interface, J. Mech. Phys. Solids 48 (10) (2000) 2183–2212, https://doi.org/10.1016/s0022-5096(99)00086-1.
[34] D.E. Spearot, K.I. Jacob, D.L. McDowell, Nucleation of dislocations from [001] bicrystal interfaces in aluminum, Acta Mater. 53 (13) (2005) 3579–3589, https://doi.org/10.1016/j.actamat.2005.04.012.
[35] P. Gupta, S. Pal, N. Yedla, Molecular dynamics based cohesive zone modeling of Al (metal)–Cu50Zr50 (metallic glass) interfacial mechanical behavior and investigation of dissipative mechanisms, Mater. Des. 105 (2016) 41–50, https://doi.org/10.1016/j.matdes.2016.05.054.
[36] T. Darden, D. York, L. Pedersen, Particle mesh Ewald: an N·log(N) method for Ewald sums in large systems, J. Chem. Phys. 98 (12) (1993) 10089–10092, https://doi.org/10.1063/1.464397.
[37] R. Bonnet, J.L. Verger-Gaugry, Couche épitaxique mince sur un substrat semi-infini: Role du désaccord paramétrique et de l'épaisseur sur les distortions élastiques, Philos. Mag. A 66 (5) (1992) 849–871, https://doi.org/10.1080/01418619208201594.
[38] A. Bourret, How to control the self-organization of nanoparticles by bonded thin layers, Surf. Sci. 432 (1–2) (1999) 37–53, https://doi.org/10.1016/s0039-6028(99)00501-4.
[39] L.H. Liang, X.M. You, H.S. Ma, Y.G. Wei, Interface energy and its influence on interface fracture between metal and ceramic thin films in nanoscale, J. Appl. Phys. 108 (8) (2010) 084317, , https://doi.org/10.1063/1.3501090.
[40] F. Ma, J.-M. Zhang, K.-W. Xu, Theoretical analysis of interface energy for unrelaxed Ag(001)/Ni(001) twist interface boundaries with MAEAM, Surf. Interface Anal. 36 (4) (2004) 355–359, https://doi.org/10.1002/sia.1782.
[41] J.R. Smith, T. Hong, D.J. Srolovitz, Metal-ceramic adhesion and the Harris functional, Phys. Rev. Lett. 72 (25) (1994) 4021–4024, https://doi.org/10.1103/PhysRevLett. 72.4021.
[42] D.M. Duffy, J.H. Harding, A.M. Stoneham, Atomistic modelling of metal-oxide interfaces with image interactions, Philos. Mag. A 67 (4) (1993) 865–882, https://doi.org/10.1080/01418619308213964.
[43] U. Scho¨nberger, O.K. Andersen, M. Methfessel, Bonding at metal-ceramic interfaces; AB initio density-functional calculations for Ti and Ag on MgO, Acta Metall. Mater. 40 (1992) S1–S10, https://doi.org/10.1016/0956-7151(92)90257-F.
[44] T. Hong, J.R. Smith, D.J. Srolovitz, Metal/ceramic adhesion: a first principles study of MgO/Al and MgO/Ag, J. Adhes. Sci. Technol. 8 (8) (1994) 837–851, https://doi.org/10.1163/156856194x00474.
[45] S. Stankic, R. Cortes-Huerto, N. Crivat, D. Demaille, J. Goniakowski, J. Jupille, Equilibrium shapes of supported silver clusters, Nanoscale 5 (6) (2013) 2448–2453, https://doi.org/10.1039/c3nr33896g.
[46] R. Benedek, M. Minkoff, L.H. Yang, Adhesive energy and charge transfer for MgO/Cu heterophase interfaces, Phys. Rev. B 54 (11) (1996) 7697–7700, https://doi.org/10.1103/PhysRevB.54.7697.
[47] X. Wu, T. Sun, R. Wang, L. Liu, Q. Liu, Energy investigations on the adhesive properties of Al/TiC interfaces: first-principles study, Physica B 449 (2014) 269–273, https://doi.org/10.1016/j.physb.2014.05.037.
[48] G. Singh, Y. Yu, F. Ernst, R. Raj, Shear strength and sliding at a metal–ceramic (aluminum–spinel) interface at ambient and elevated temperatures, Acta Mater. 55 (9) (2007) 3049–3057, https://doi.org/10.1016/j.actamat.2007.01.008.
[49] J.P. Hirth, J. Lothe, Theory of Dislocations, Krieger Publishing Company, Malabar, FI, 1982.
[50] J. Wang, A. Misra, An overview of interface-dominated deformation mechanisms in metallic multilayers, Curr. Opin. Solid State Mater. Sci. 15 (1) (2011) 20–28, https://doi.org/10.1016/j.cossms.2010.09.002.
[51] S. Shao, J. Wang, A. Misra, R.G. Hoagland, Spiral patterns of dislocations at nodes in (111) semi-coherent FCC interfaces, Sci. Rep. 3 (2013) 2448, https://doi.org/10.1038/srep02448.
[52] J. Wang, R.G. Hoagland, J.P. Hirth, A. Misra, Atomistic simulations of the shear strength and sliding mechanisms of copper-niobium interfaces, Acta Mater. 56 (13) (2008) 3109–3119, https://doi.org/10.1016/j.actamat.2008.03.003.
[53] H.X. Xie, C.Y. Wang, T. Yu, Motion of misfit dislocation in an Ni/Ni3Al interface: a molecular dynamics simulations study, Modell. Simul. Mater. Sci. Eng. 17 (5) (2009) 055007, , https://doi.org/10.1088/0965-0393/17/5/055007.